

Hilbert Curve Based Molecular Sequence Analysis

Sarwan Ali^{1*}, Tamkanat E Ali^{2*}, Imdad Ullah Khan², and Murray Patterson¹

¹Department of Computer Science, Georgia State University, Atlanta, Georgia, USA

²Department of Computer Science, Lahore University of Management Sciences, Lahore, Pakistan

sali85@student.gsu.edu, 20100159@lums.edu.pk,

imdad.khan@lums.edu.pk, mpatterson30@gsu.edu

*Equal Contribution

Abstract. Accurate molecular sequence analysis is a key task in the field of bioinformatics. To apply molecular sequence classification algorithms, we first need to generate the appropriate representations of the sequences. Traditional numeric sequence representation techniques are mostly based on sequence alignment that faces limitations in the form of lack of accuracy. Although several alignment-free techniques have also been introduced, their tabular data form results in low performance when used with Deep Learning (DL) models compared to the competitive performance observed in the case of image-based data. To find a solution to this problem and to make Deep Learning (DL) models function to their maximum potential while capturing the important spatial information in the sequence data, we propose a universal Hilbert curve-based Chaos Game Representation (CGR) method. This method is a transformative function that involves a novel Alphabetic index mapping technique used in constructing Hilbert curve-based image representation from molecular sequences. Our method can be globally applied to any type of molecular sequence data. The Hilbert curve-based image representations can be used as input to sophisticated vision DL models for sequence classification. The proposed method shows promising results as it outperforms current state-of-the-art methods by achieving a high accuracy of 94.5% and an F1 score of 93.9% when tested with the CNN model on the lung cancer dataset. This approach opens up a new horizon for exploring molecular sequence analysis using image classification methods.

Keywords: Chaos Game Representation, Hilbert Curve, Protein Sequences

1 Introduction

With the rapid increase in biological sequence data, there is a growing challenge of effective data analysis, mining, and visualization. Molecular Sequence analysis plays a crucial role in disease detection, drug discovery, etc. To analyze molecular sequences such as DNA, Proteins, etc using ML and DL-based algorithms there is a need to generate appropriate representations of their basic units including nucleotides and amino acids.

The numeric vector-based embeddings [13] have been widely used to form molecular sequence representations and have shown promising results when used with ML

classifiers but when Deep Learning classification models such as Neural networks (NN) are applied to the numeric vectors they perform suboptimally as NN models struggle with tabular data [25] due to issues like feature sparsity, varying scales, and the lack of spatial correlations. As a solution image-based molecular sequence embeddings [1] were introduced that show improved performance when used with DL-based classification models. One of the most widely used image-based representation methods is based on Chaos game representation (CGR) [16] which is a groundbreaking invention in the field of graphical bioinformatics and has gained increasing popularity as it has proved to be successful in the effective image-based encoding of biological sequence features for the accurate application of Deep learning algorithms as it effectively maps a sequence to 2-dimensional space. It has also proved to be a powerful tool for alignment-free sequence comparison. The CGR is based on the concept of the Markov chain and it allows a unique representation of a sequence. On the other hand Frequency matrix representation (FCGR) which is an extension of (CGR), takes sequences of different lengths as input and transforms them into equal-sized images or matrices.

Despite the promising performance of Deep Learning (DL) classification models when used with these image-based sequence representations, most existing methods face a major limitation in accurately capturing all the important information preserved in the data while keeping the accuracy intact as they only consider sequence information regardless of spatial information [34]. To provide a solution to this challenge Hilbert curve-based image representations [33] were introduced to represent molecular sequences in a manner that not only helped perform significantly well in DL-based classification tasks but also was successful in capturing the important spatial information in the sequence data. A Hilbert curve [23] is a continuous fractal space-filling curve that maps 1-dimensional sequences to a two-dimensional plane. Hilbert curve is considered better than other space-filling curves such as z-order and Peano curves because it has much better spatial cohesion [7], spatial continuity, and self-similarity [5]. Hilbert curve has been widely used for visualizing genomic data [20]. These current Hilbert curve-based representation methods fail to provide a universal solution as their encoding is specific to the type of molecular sequence used. To overcome this limitation we propose a universal Hilbert curve-based Chaos Game Representation (CGR) method that involves a unique Alphabetic index mapping technique used in constructing Hilbert curve-based image representations from molecular sequences. This technique can be globally applied to any type of molecular sequence. These Hilbert curve-based representations are further used as input to DL models for sequence classification. Our study presents the following key contributions:

- We introduce a novel universal Hilbert curve-based Chaos Game Representation (CGR) method for converting molecular sequences into image representations. It involves a novel Alphabetic index mapping technique used in constructing Hilbert curve-based image representation from molecular sequences enabling the application of advanced vision deep learning models for sequence classification tasks.
- Our approach is rigorously tested on various molecular sequence datasets, showcasing significant improvements in predictive performance compared to traditional methods.

- The proposed methodologies are not limited to the molecular sequences but are also applicable to other sequence datasets from the NLP domain, illustrating the versatility and broad impact of our work.

2 Related Work

Several methods have been used to generate numeric vector-based embeddings to represent molecular sequences such as Feature Engineering, Natural Language Processing (NLP), Neural Networks, and Kernel-based methods. Feature Engineering-based embedding generation methods is a well-explored field with significant discoveries including PWM2Vec [3] that involves weight assignment strategy for each amino acid in a k -mer based on its position for generating numeric representation, some prominent peptide descriptors include amino acid composition (AAC) [6], Composition of k -spaced amino acid group pairs (CKSAAGP) [30], pseudo amino acid composition (PAAC) [4] and physicochemical features (PHYC). In another research [21], a combination of such descriptors is used for anti-CoV peptides classification. Neural Network-based molecular sequence embeddings have been the target of extensive research. Autoencoder has been used by multiple researchers for generating molecular sequence representations [10]. Natural Language Processing (NLP) has gained popularity in the field of bioinformatics. NLP-based methods have been widely used for molecular sequence embedding generation, some recent works include SeqVec [12], PRoBERTa [19], MSA-transformer [22], and ESM2 [28]. Other than numeric representations, image-based representations are also used to represent molecular sequences which are further used as input to DL-based image classification algorithms. Most widely used Image-based representations of molecular sequences involve Chaos game representation strategy such as Spike2CGR [18] which converts spike sequences to graphical (image) representation, FCGR [11] converts DNA sequences to images, SARS-CoV-2 lineages, strains and recombinants are classified using CGR based representations [29]. Hilbert curve-based image representations [33] have also been used to represent molecular sequences.

3 Proposed Approach

In this section, we present the details of our proposed universal Hilbert curve-based Chaos Game Representation (CGR) method for transforming biological sequences into image representations suitable for deep learning classification. The core idea is to map one-dimensional biological sequences onto a two-dimensional plane using a Hilbert curve, which preserves spatial locality and captures essential features of the sequences.

The Hilbert curve is a continuous fractal space-filling curve [23], which is used for mapping data from a one-dimensional space to a two-dimensional space that preserves locality. This essentially means that the points that are close in the one-dimensional space remain close in the two-dimensional mapping. This property is particularly advantageous for encoding molecular sequences because it maintains the proximity of sequence elements in the image representation.

Mathematically, the Hilbert curve of order p in N dimensions can be defined recursively. The total number of points Θ on the curve is given by $\Theta = 2^{p*N}$, where p is the

number of iterations (or the order of the curve), and N is the number of dimensions. Since we are generating the 2-dimensional image, the value for N is taken as 2. To generate the images of standard size (i.e. 64×64), we use $p = 6$ to get $2^6 \times 2^6 = 64 \times 64$ dimensional image for any given sequence. Note that when p represents the number of iterations in constructing the Hilbert curve, the dimensions of the resulting image are determined by the expression $2^p \times 2^p$. Each increment in p leads to an exponential increase in the size of the image, allowing the curve to fill more space and represent more complex data or patterns effectively.

Hilbert Curve Computation Given a set of biological sequences $S = \{s_1, s_2, \dots, s_n\}$, where each sequence s_i consists of characters from the alphabet set A , we generate Hilbert curve-based image representations using the Algorithm 1. The goal is to map each character in s_i to a unique point on the Hilbert curve, resulting in an image representation of the sequence. The flow diagram is presented in Figure 1, which gives a bigger picture of the steps involved in our proposed approach.

Alphabetic Index Mapping: We define an alphabetic index mapping function $\text{IndexMapping}(c)$ in Algorithm 2 that assigns a unique integer index I to each character c in the alphabet A :

$$I = \text{IndexMapping}(c), c \in A \quad (1)$$

This mapping ensures that each character is represented by a distinct numerical value (see Step (b) in Figure 1).

Distance Calculation: For each character c in the sequence s_i , we calculate a normalized distance D along the Hilbert curve as shown in line number 8 of Algorithm 1 (also see Step (c) in Figure 1):

$$D = \frac{I}{L} * \Theta \quad (2)$$

where L is the length of the sequence s_i , and Θ is the total number of points on the Hilbert curve. This equation scales the index I proportionally to the sequence length and maps it onto the range of the Hilbert curve.

Remark 1. The combination of index mapping and distance calculation ensures a bijective relationship between sequence characters and points on the Hilbert curve within the resolution defined by p . This means each character maps to a unique point, preventing information loss.

Computing Hilbert Curve Coordinates: The next step involves converting the distance D into two-dimensional coordinates (x, y) on the Hilbert curve using Algorithm 3 (also see Step (d) in Figure 1). This is achieved through a series of transformations involving binary representations and Gray codes.

Binary Representation: We convert the distance D into a binary number with $n = p \times N$ bits as shown in line number 2 and 3 of Algorithm 3:

$$\text{Bits} = \text{Binary}(D) = b_{n-1}b_{n-2} \dots b_0 \quad (3)$$

Bit Interleaving: We separate the bits into even and odd indices to form the coordinate components as shown in lines number 7 and 8 of Algorithm 3:

$$EvenIdxBits = b_{n-1}b_{n-3} \dots \quad (4)$$

$$OddIdxBits = b_{n-2}b_{n-4} \dots \quad (5)$$

These binary sequences are then converted back to decimal form to obtain preliminary coordinate values as shown in line numbers 14 and 16 of Algorithm 3:

$$x_{raw} = Decimal(EvenIdxBits) \quad (6)$$

$$y_{raw} = Decimal(OddIdxBits) \quad (7)$$

Gray Code Transformation: We apply the Gray code transformation to the coordinate components to minimize bit changes between successive values, preserving spatial locality. We apply this transformation by calling the function 'GENERATEGRAYCODE()' in line number 18 of Algorithm 3. The function GENERATEGRAYCODE() is defined in Algorithm 4 and the following equations:

$$x_{gray} = x_{raw} \oplus (x_{raw} \gg 1) \quad (8)$$

$$y_{gray} = y_{raw} \oplus (y_{raw} \gg 1) \quad (9)$$

where \oplus denotes the bitwise XOR operation and \gg denotes a bitwise right shift.

Algorithm 4 applies Global np -fold Gray code [27] to all bits of each integer representing distance along the Hilbert Curve at once yielding a result that is quite close to the desired spatial coordinates.

Coordinate Refinement: During the process of Gray Code transformation large number of exchanges and inversions are conducted resulting in an over-transformed length. The excess transformation is undone using the function 'REFINING()' in line 19 of Algorithm 3 that works according to Algorithm 5 that refines the Gray code to obtain the final Hilbert curve coordinates (x, y) . This involves inverting the Gray code transformation:

$$x = InverseGrayCode(x_{gray}) \quad (10)$$

$$y = InverseGrayCode(y_{gray}) \quad (11)$$

The inverse Gray code transformation is performed iteratively:

$$\begin{aligned} x &= x_{gray} \\ \text{For } i &= n - 2 \text{ to } 0 : \\ x_i &= x_i \oplus x_{i+1} \end{aligned} \quad (12)$$

The same above process applies to y_{gray} to obtain y . The equations above conduct the exchanges and inversions needed to transform Gray Code into the desired coordinates. The refined output (x, y) gives us the Hilbert Curve point coordinates.

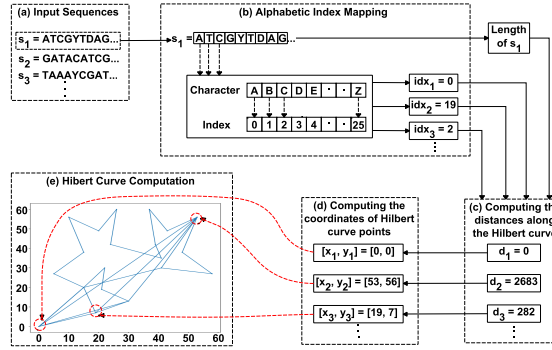


Fig. 1: Flow diagram for the proposed method.

Algorithm 1 Hilbert Curve Computation

Input: Set of Biological Sequences (S), Number of Iterations p , Number of Dimensions N , Alphabets (A)
Output: Hilbert Curve Coordinates (H)

```

1: function COMPUTEHILBERTCURVE( $S, p, N$ )
2:    $H \leftarrow []$ 
3:    $\Theta = 2^{(p \times N)}$  ▷ Compute number of unit hypercubes using  $p = 6$  and  $N = 2$ 
4:   for  $s_1$  in  $S$  do
5:      $L \leftarrow \text{Length}(s_1)$ 
6:     for  $char$  in  $s_1$  do
7:        $Index \leftarrow \text{INDEXMAPPING}(char, A)$ 
8:        $D \leftarrow \frac{Index}{L} * \Theta$  ▷ Compute distances along Hilbert curve
9:        $Coordinates \leftarrow \text{PointfromDistance}(D)$  ▷ Single Hilbert curve point coordinates
10:       $H.append(Coordinates)$ 
11:    end for
12:  end for
13:  return  $H$ 
14: end function

```

Algorithm 2 Alphabetic Index Mapping

Input: Biological Sequence single character (c), Alphabets (A)
Output: Index (I)

```

1: function INDEXMAPPING( $c, A$ )
2:
3:   for  $a$  in  $A$  do
4:     if  $a = c$  then
5:        $I = A.index(c)$  ▷ Find the alphabetic index of single sequence character
6:     end if
7:   end for
8:   return  $I$ 
9: end function

```

3.1 Mathematical Justification

Gray Code Utilization: Gray codes are employed to minimize the Hamming distance between successive integer values, which translates to minimal movement between adjacent points on the Hilbert curve. This is crucial for maintaining the continuity and smoothness of the curve, and it enhances the preservation of sequential information in the image representation.

Algorithm 3 Distance to Hilbert Curve Point

Input: Distance along Hilbert Curve (D), Number of Iterations (p)
Output: Point (ϕ)

```

1: function POINTFROMDISTANCE( $D$ )
2:   NumBits =  $N * p$  ▷ Number of bits
3:   Bits = Binary( $D$ ) ▷ Distance to Binary string representation of  $N * p$  bits
4:   OddIdxBits ← []
5:   EvenIdxBits ← []
6:   Components ← []
7:   for  $i$  in range(0, LenBits) do
8:     if  $i \% 2 = 0$  then
9:       EvenIdxBits.append(Bits[ $i$ ])
10:    else if  $i \% 2 = 1$  then
11:      OddIdxBits.append(Bits[ $i$ ])
12:    end if
13:  end for
14:  EvenIdxDeci = Decimal(EvenIdxBits)
15:  Components.append(EvenIdxDeci)
16:  OddIdxDeci = Decimal(OddIdxBits)
17:  Components.append(OddIdxDeci)
18:  GrayCode ← GENERATEGRAYCODE(Components,  $n$ )
19:   $\phi$  ← REFINING(GrayCode,  $p$ )
20:  return  $\phi$ 
21: end function

```

Algorithm 4 Gray Code Computation

Input: Components (C), n
Output: Gray Code (γ)

```

1: function GENERATEGRAYCODE( $C$ )
2:    $r = C[n-1] \gg 1$  ▷ Right shift
3:   for  $i$  in range( $n-1, 0, -1$ ) do
4:      $C[i] \leftarrow C[i] \oplus C[i-1]$  ▷ Bitwise XOR between two consecutive bits
5:   end for
6:    $C[0] \leftarrow C[0] \oplus r$ 
7:    $\gamma \leftarrow C$ 
8:   return  $\gamma$ 
9: end function

```

Algorithm 5 Refining

Input: Gray Code Integers (g), Number of Iterations (p)
Output: Point (β)

```

1: function REFINING( $g$ )
2:    $q = 2$ 
3:    $z = 2 \ll (p-1)$ 
4:   while  $q \neq z$  do
5:      $w = q - 1$ 
6:     for  $i$  in range( $n-1, -1, -1$ ) do
7:       if  $g[i] \& q$  then ▷ Check if the specific bit that is ON in  $q$  is also ON in  $g[i]$ 
8:          $g[0] = g[0] \oplus w$  ▷ Invert low bits of  $g[0]$ 
9:       else
10:         $t = (g[0] \oplus g[i]) \& w$ 
11:         $g[0] = g[0] \oplus t$  ▷ Exchange low bits of  $g[0]$  and  $g[i]$ 
12:         $g[i] = g[i] \oplus t$ 
13:      end if
14:    end for
15:     $q = q \ll 1$ 
16:  end while
17:   $\beta \leftarrow g$ 
18:  return  $\beta$ 
19: end function

```

Refinement Process: The refinement step corrects the over-transformation caused by the global Gray code application. By performing inversions and exchanges in a backward pass through the higher-order bits, we ensure that the final coordinates accurately reflect the intended mapping.

3.2 Collision Guarantee

The Hilbert curve is a space-filling curve, and thus, as $p \rightarrow \infty$, the curve becomes denser, filling all points in the space. For a finite p , the guarantee is that the curve will cover all unit hypercubes without any overlap within the resolution limit set by $\Theta = 2^{p \times N}$.

3.3 Upper Bound on Uniqueness

Since the Hilbert curve is injective for any given resolution, there is no loss of information within the resolution constraints. As long as the number of unit hypercubes exceeds the sequence length (i.e., $\Theta > L$), the curve guarantees a unique mapping of characters to curve points. If $\Theta \leq L$, multiple characters may map to the same spatial location, leading to potential loss of information.

4 Experimental Setup

To compare results for proposed method with existing approaches, we divided the baselines into vector-based and image-based methods. For vector-based, we use one hot encoding OHE [14], Spike2Vec [2], Minimizer spectrum [8], Spaced k -mers spectrum [26], PWM2Vec [3], Wasserstein Distance Guided Representation Learning (WDGRL) [24], Auto-Encoder [32], and pre-trained LLM known as SeqVec [12]. For image-based baselines, we use Frequency Chaos Game Representation (FCGR) [15], Spike2CGR [18], and Random Chaos Game Representation (RANDOMCGR) [17].

In this study, we employed two categories of classifiers: vector-based and image-based. In the vector-based setting, we use the standard nearest neighbor classifier, which is well-known and traditionally used in the literature for such tasks. For the image-based classifiers, we use various deep-learning architectures, including 1, 2, and 3 layers of Convolutional Neural Network (CNN), Visual Geometry Group (VGG19), ResNet50, EfficientNet, and DenseNet. For the parameters of the DL models, we selected values for batch size, epochs, and learning rate as 64, 10, and 0.003, respectively. For the optimizer, we use ADAM. For hyperparameter tuning, we use a standard cross-validation setting. To evaluate the performance of the classifiers, we use average accuracy, precision, recall, weighted F1, Macro F1, ROC-AUC, and training runtime.

The dataset used in this study consists of peptide sequences classified based on their anticancer activity against breast and lung cancer cell lines [9]. These anti-cancer peptides (ACP) are categorized into four groups: "very active," "moderately active," "experimental inactive," and "virtual inactive," reflecting their varying levels of anticancer effectiveness. This makes it a 4-class classification problem. The breast cancer dataset contains 949 peptide sequences, while the lung cancer dataset includes 901 sequences.

The peptide lengths vary across categories, with the minimum sequence length being 5 and the maximum 38. On average, sequences range from 14.5 to 20.7 amino acids long, depending on their activity level. This distribution ensures a diverse set of peptide lengths and activity profiles, facilitating a robust evaluation of the proposed method. For data splitting, we use standard 80 percent for training and 20 percent for testing (i.e. held-out set). From the training data, 10 percent is used for validation. All experiments are conducted on an Intel i5 processor (2.40 GHz) and 32 GB of RAM. The operating system used is Windows 10, and the code is implemented using Python.

5 Results And Discussion

In this section, we present and discuss the results of our classification experiments on both the breast cancer dataset and the second dataset.

The results for the breast cancer ACPs are reported in Table 1. The vector-based methods, which are used as traditional baselines (other than Auto-Encoder and WD-GRL), show sub-optimal performance overall. For the Auto-Encoder, we can observe a higher predictive performance, achieving an accuracy of 83.2%, a weighted F1 score of 80.4%, and a ROC-AUC of 64.5%. This highlights the utility of feature learning in extracting meaningful representations from the sequences. WDGRL, a domain adaptation approach, provides comparatively higher performance with an accuracy of 79.4%. However, it fell short in terms of F1 macro and ROC-AUC metrics, indicating the potential misalignment between the source and target domains in this scenario.

The image-based methods showed a wide range of performance across different CNN architectures. The proposed method consistently outperformed other image-based methods, achieving the highest accuracy of 89.5%, precision of 86.9%, recall of 89.5%, and an F1-weighted score of 88.1% when using the 1-Layer CNN architecture. This indicates that our sequence-to-image transformation approach combined with a simple CNN model was effective in capturing the underlying patterns in the molecular sequence data. Among other CNN architectures, 4-Layer CNN also provided competitive results, with an accuracy of 87.4% and an F1-weighted score of 86.7%, while the 3-Layer CNN achieved slightly lower performance. Interestingly, EfficientNet shows poor performance with accuracies as low as 8.4%, suggesting that the deeper networks struggled to generalize well on the molecular image data. In general, the CNN-based models, especially the simpler architectures like the 1-Layer CNN, excelled at the task of sequence classification, likely due to their ability to capture both local and global patterns in the image representation of the sequences.

For the lung cancer dataset results, as shown in Table 2, the vector-based methods also present suboptimal performance for methods like PWM2Vec. The Auto-Encoder, however, delivered improved results, with an accuracy of 91.0%, a weighted F1 score of 90.8%, and a ROC-AUC of 77.1%, suggesting its effectiveness in capturing important sequence characteristics for lung cancer ACPs. The WDGRL, while providing an accuracy of 86.2%, exhibited lower scores in F1 macro and ROC-AUC, reinforcing the challenge of aligning the source and target domains effectively for this specific dataset.

The image-based methods displayed a broader range of outcomes across different CNN models, similar to the breast cancer results. Our proposed method, employing the

Method	Algorithm	ML/DL Model	Acc. \uparrow	Prec. \uparrow	Recall \uparrow	F1 weigh. \uparrow	F1 Macro \uparrow	ROC- AUC \uparrow	Train. runtime (sec.) \downarrow	
Vector Based	OHE	-	0.609	0.853	0.609	0.676	0.395	0.678	0.069	
	Spike2Vec	-	0.241	0.298	0.241	0.212	0.200	0.550	0.133	
	Minimizer	-	0.577	0.807	0.577	0.635	0.332	0.616	0.149	
	Spaced k-mer	-	0.276	0.460	0.276	0.253	0.216	0.559	1.036	
	PWM2Vec	-	0.199	0.808	0.199	0.221	0.190	0.541	0.618	
	WDGRL	-	0.794	0.715	0.794	0.730	0.270	0.518	0.016	
	Auto-Encoder	-	0.832	0.802	0.832	0.804	0.431	0.645	0.067	
	SeqVec	-	0.674	0.819	0.674	0.725	0.389	0.651	22.253	
	FCGR	1 Layer CNN		0.863	0.831	0.863	0.844	0.490	0.677	5410.357
		3 Layer CNN		0.800	0.640	0.800	0.711	0.222	0.500	52147.851
4 Layer CNN			0.831	0.735	0.831	0.779	0.329	0.586	56873.749	
VGG19 (pre-trained)			0.803	0.684	0.803	0.720	0.243	0.509	51234.241	
RESNET50 (pre-trained)			0.800	0.642	0.800	0.712	0.222	0.501	49715.758	
Efficient Net			0.089	0.008	0.089	0.014	0.041	0.500	8731.614	
Dense Net			0.116	0.013	0.116	0.024	0.052	0.500	11482.259	
Spike2CGR		1 Layer CNN		0.783	0.613	0.783	0.687	0.219	0.500	6547.979
		3 Layer CNN		0.783	0.612	0.783	0.687	0.219	0.500	55419.449
		4 Layer CNN		0.783	0.612	0.783	0.687	0.219	0.500	56482.458
	VGG19 (pre-trained)		0.765	0.650	0.765	0.650	0.200	0.500	49851.852	
	RESNET50 (pre-trained)		0.770	0.559	0.770	0.654	0.198	0.500	50179.716	
	Efficient Net		0.085	0.005	0.085	0.009	0.008	0.500	9812.984	
	Dense Net		0.116	0.011	0.116	0.022	0.050	0.500	10248.154	
	RandomCGR	1 Layer CNN		0.792	0.638	0.792	0.707	0.221	0.497	4982.864
		3 Layer CNN		0.800	0.640	0.800	0.711	0.222	0.500	53214.341
		4 Layer CNN		0.800	0.640	0.800	0.711	0.222	0.500	64128.387
VGG19 (pre-trained)			0.800	0.640	0.800	0.711	0.222	0.500	53214.524	
RESNET50 (pre-trained)			0.800	0.640	0.800	0.711	0.222	0.500	55654.851	
Efficient Net			0.028	0.002	0.028	0.004	0.027	0.500	9547.759	
Dense Net			0.095	0.011	0.095	0.010	0.095	0.500	10247.751	
Ours		1 Layer CNN		0.895	0.869	0.895	0.881	0.521	0.725	2136.810
		3 Layer CNN		0.842	0.834	0.842	0.838	0.429	0.672	13544.320
		4 Layer CNN		0.874	0.861	0.874	0.867	0.476	0.705	13044.890
	VGG19 (pre-trained)		0.863	0.774	0.863	0.815	0.407	0.675	25081.410	
	RESNET50 (pre-trained)		0.853	0.837	0.853	0.841	0.465	0.690	11202.436	
	Efficient Net		0.084	0.007	0.084	0.013	0.039	0.500	3057.010	
Dense Net		0.800	0.640	0.800	0.711	0.222	0.500	2819.100		

Table 1: Classification results for **Breast Cancer dataset**.

1-Layer CNN, outperformed all other approaches with an accuracy of 94.5%, precision of 93.8%, recall of 94.5%, and an F1-weighted score of 93.9%. This demonstrates the strength of our sequence-to-image transformation technique in revealing patterns within the lung cancer molecular sequence data. The 3-Layer CNN and 4-Layer CNN also showed promising results, however, deeper architectures such as EfficientNet struggled again, showing a low accuracy of 6.1%. Overall, the simpler CNN models, particularly the 1-Layer CNN, performed exceptionally well, suggesting that less complex architectures are better suited for capturing informative features from molecular sequence images in the lung cancer dataset. According to Occam’s razor [31], the simplest solution is often the best one. A 1-layer CNN may strike the optimal balance between model simplicity and learning capability for this particular task, where the sequence-to-image transformation provides enough meaningful features that don’t require deeper processing, leading to better generalization on unseen data.

6 Conclusion

In this work, we proposed a novel approach for classifying molecular sequences by transforming them into images using the sequence-to-image transformation technique, called the Hilbert curve. The results demonstrate the potential of our method in capturing intricate patterns within molecular sequence data, particularly when coupled with

Method	Algorithm	ML/DL Model	Acc. ↑	Prec. ↑	Recall ↑	F1 weigh. ↑	F1 Macro ↑	ROC-AUC ↑	Train. runtime (sec.) ↓	
Vector Based	OHE	-	0.804	0.907	0.804	0.835	0.537	0.781	0.117	
	Spike2Vec	-	0.877	0.919	0.877	0.883	0.590	0.790	0.590	
	Minimizer	-	0.858	0.835	0.858	0.840	0.455	0.681	0.837	
	Spaced k-mer	-	0.883	0.871	0.883	0.862	0.530	0.699	21.594	
	PWM2Vec	-	0.452	0.842	0.452	0.511	0.335	0.614	0.931	
	WDGRL	-	0.862	0.820	0.862	0.822	0.360	0.583	0.050	
	Auto-Encoder	-	0.910	0.908	0.910	0.906	0.602	0.771	0.090	
	SeqVec	-	0.886	0.882	0.886	0.878	0.604	0.761	33.326	
	FCGR	1 Layer CNN	-	0.910	0.911	0.910	0.910	0.582	0.755	5023.028
		3 Layer CNN	-	0.930	0.925	0.930	0.929	0.681	0.810	41247.742
4 Layer CNN		-	0.909	0.912	0.909	0.911	0.587	0.751	42215.749	
VGG19 (pre-trained)		-	0.921	0.919	0.921	0.918	0.600	0.776	59713.943	
RESNET50 (pre-trained)		-	0.915	0.918	0.915	0.914	0.598	0.777	49853.749	
Efficient Net		-	0.101	0.012	0.101	0.023	0.059	0.500	9024.137	
Dense Net		-	0.231	0.030	0.231	0.031	0.061	0.500	9851.749	
Spike2CGR		1 Layer CNN	-	0.833	0.779	0.833	0.764	0.291	0.551	5987.149
		3 Layer CNN	-	0.831	0.780	0.831	0.749	0.587	0.548	58745.217
		4 Layer CNN	-	0.825	0.771	0.825	0.751	0.585	0.545	59412.743
	VGG19 (pre-trained)	-	0.805	0.852	0.805	0.851	0.573	0.544	50125.126	
	RESNET50 (pre-trained)	-	0.837	0.799	0.837	0.843	0.555	0.541	51249.354	
	Efficient Net	-	0.054	0.011	0.054	0.015	0.019	0.509	8712.258	
	Dense Net	-	0.324	0.021	0.324	0.030	0.095	0.507	11423.017	
	RandomCGR	1 Layer CNN	-	0.854	0.798	0.854	0.814	0.314	0.588	5024.749
		3 Layer CNN	-	0.853	0.791	0.853	0.801	0.302	0.580	51249.149
		4 Layer CNN	-	0.852	0.784	0.852	0.795	0.310	0.567	67418.249
VGG19 (pre-trained)		-	0.892	0.714	0.892	0.769	0.297	0.524	60214.143	
RESNET50 (pre-trained)		-	0.890	0.701	0.890	0.755	0.294	0.532	51478.215	
Efficient Net		-	0.035	0.003	0.035	0.006	0.032	0.500	8745.149	
Dense Net		-	0.099	0.015	0.099	0.014	0.098	0.500	11427.137	
Ours		1 Layer CNN	-	0.945	0.938	0.945	0.939	0.664	0.791	1648.930
		3 Layer CNN	-	0.906	0.915	0.906	0.908	0.563	0.758	16365.380
		4 Layer CNN	-	0.912	0.909	0.912	0.909	0.534	0.729	15161.590
	VGG19 (pre-trained)	-	0.917	0.888	0.917	0.898	0.490	0.683	19264.990	
	RESNET50 (pre-trained)	-	0.906	0.909	0.906	0.900	0.551	0.713	15041.838	
	Efficient Net	-	0.061	0.876	0.061	0.027	0.031	0.503	5037.620	
Dense Net	-	0.873	0.762	0.873	0.814	0.233	0.500	3961.028		

Table 2: Classification results for **Lungs Cancer dataset**.

CNN architectures. Future work could explore integrating advanced domain adaptation techniques to further enhance model generalization across different datasets, as well as experimenting with hybrid architectures that combine the strengths of vector-based and image-based approaches.

References

1. Abadi, S., et al.: Walkim: Compact image-based encoding for high-performance classification of biological sequences using simple tuning-free cnns. *Plos one* **17**(4) (2022)
2. Ali, S., Patterson, M.: Spike2vec: An efficient and scalable embedding approach for covid-19 spike sequences. In: *IEEE International Conference on Big Data*. pp. 1533–1540 (2021)
3. Ali, S., et al.: PWM2Vec: An efficient embedding approach for viral host specification from coronavirus spike sequences. *Biology* **11**(3), 418 (2022)
4. Beltrán, J.F., et al.: Multitoxpred 1.0: a novel comprehensive tool for predicting 27 classes of protein toxins using an ensemble ml approach. *BMC bioinformatics* **25**(1), 148 (2024)
5. Cardona, L.F., Múnera, L.E.: Self-similarity of space filling curves. *Ingeniería y competitividad* **18**(2), 113–124 (2016)
6. Fu, H., et al.: Acep: improving antimicrobial peptides recognition through automatic feature fusion and amino acid embedding. *BMC genomics* **21**, 1–14 (2020)
7. Ghosh, S., Bhattacharya, S.: Hilbert curve based steganographic scheme for large data hiding. In: *International Conference on Image Information Processing*. pp. 91–96 (2015)
8. Giroto, S., Pizzi, C., Comin, M.: Metaprob: accurate metagenomic reads binning based on probabilistic sequence signatures. *Bioinformatics* **32**(17), i567–i575 (2016)

9. Grisoni, et al.: 'de novo design of anticancer peptides by ensemble artificial neural networks'. 'Journal of Molecular Modeling' **'25'**(5), '112' ('2019')
10. Hadipour, H., et al.: Deep clustering of small molecules at large-scale via variational autoencoder embedding and k-means. *BMC bioinformatics* **23**(Suppl 4), 132 (2022)
11. Halder, A., Piyush, Mathew, B., Sengupta, D.: Improved python package for dna sequence encoding using frequency chaos game representation. *bioRxiv* pp. 2024-04 (2024)
12. Heinzinger, M., et al.: Modeling aspects of the language of life through transfer-learning protein sequences. *BMC bioinformatics* **20**, 1–17 (2019)
13. Iuchi, H., et al.: Representation learning applications in biological sequence analysis. *Computational and Structural Biotechnology Journal* **19**, 3198–3208 (2021)
14. Kuzmin, K., et al.: Machine learning methods accurately predict host specificity of coronaviruses based on spike sequences alone. *BBRC* **533**(3), 553–558 (2020)
15. Löchel, H.F., Eger, D., Sperlea, T., Heider, D.: Deep learning on chaos game representation for proteins. *Bioinformatics* **36**(1), 272–279 (2020)
16. Löchel, H.F., Heider, D.: Chaos game representation and its applications in bioinformatics. *Computational and Structural Biotechnology Journal* **19**, 6263–6271 (2021)
17. Murad, T., et al.: A new direction in membranolytic anticancer peptides classi.: Combining spaced k-mers with chaos game rep.. *Procedia Computer Science* **222**, 666–675 (2023)
18. Murad, T., et al.: Spike2CGR: an efficient method for spike sequence classification using chaos game representation. *Machine Learning* **112**(10), 3633–3658 (2023)
19. Nambiar, A., et al.: Transforming the language of life: transformer neural networks for protein prediction tasks. In: *ACM-BCB*. pp. 1–8 (2020)
20. Nusrat, S., Harbig, T., Gehlenborg, N.: Tasks, techniques, and tools for genomic data visualization. In: *Computer Graphics Forum*. vol. 38, pp. 781–805. Wiley Online Library (2019)
21. Pang, Y., et al.: Identifying anti-coronavirus peptides by incorporat. different negative datasets and imbalanced learn. strategies. *Briefings in bioinformatics* **22**(2) (2021)
22. Rao, R.M., et al.: Msa transformer. In: *International Conference on Machine Learning*. pp. 8844–8856 (2021)
23. Sagan, H.: Hilbert's space-filling curve. In: *Space-filling curves*. pp. 9–30 (1994)
24. Shen, J., Qu, Y., Zhang, W., Yu, Y.: Wasserstein distance guided representation learning for domain adaptation. In: *AAAI conference on artificial intelligence* (2018)
25. Shwartz-Ziv, R., Armon, A.: Tabular data: Deep learning is not all you need. *Information Fusion* **81**, 84–90 (2022)
26. Singh, R., Sekhon, A., et al.: Gakco: a fast gapped k-mer string kernel using counting. In: *Joint ECML and Knowledge Discovery in Databases*. pp. 356–373 (2017)
27. Skilling, J.: Programming the hilbert curve. In: *AIP Conference Proceedings*. vol. 707, pp. 381–387. American Institute of Physics (2004)
28. Susanty, M., et al.: Classifying alkaliphilic proteins using embeddings from protein language model. *Computers in Biology and Medicine* **173**, 108385 (2024)
29. Thind, A.S., Sinha, S.: Using chaos-game-representation for analysing the sars-cov-2 lineages, newly emerging strains and recombinants. *Current Genomics* **24**(3), 187 (2023)
30. Usman, M., Khan, S., Lee, J.A.: Afp-lse: Antifreeze proteins prediction using latent space encoding of composition of k-spaced amino acid pairs. *Scientific Reports* **10**(1), 7197 (2020)
31. Walsh, D.: Occam's razor: A principle of intellectual elegance. *American Philosophical Quarterly* **16**(3), 241–244 (1979)
32. Xie, J., Girshick, R., Farhadi, A.: Unsupervised deep embedding for clustering analysis. In: *International conference on machine learning*. pp. 478–487 (2016)
33. Yin, B., Balvert, M., Zambrano, D., Schönhuth, A., Bohte, S.: An image representation based convolutional network for dna classification. *arXiv preprint arXiv:1806.04931* (2018)
34. Zhang, M., Hu, Y., Zhu, M.: Epishilbert: Prediction of enhancer-promoter interactions via hilbert curve encoding and transfer learning. *Genes* **12**(9), 1385 (2021)